



Advancing refractory high entropy alloy development with AI-predictive models for high temperature oxidation resistance

Stéphane Gorsse^{a,*,**}, Wei-Chih Lin^{a,b}, Hideyuki Murakami^c, Gian-Marco Rignanese^{d,e}, An-Chou Yeh^{b,f,*}

^a University Bordeaux, CNRS, Bordeaux INP, ICMCB, UMR 5026, Pessac F-33600, France

^b Department of Materials Science and Engineering, National Tsing Hua University, 101, Sec. 2, Kuang-Fu Road, Hsinchu 30013, Taiwan

^c Research Center for Structural Materials, National Institute for Materials Science, 1-2-1 Sengen, Tsukuba 305-0047, Japan

^d UCLouvain, Institute de la Matière Condensée et des Nanosciences (IMCN), Chemin des Étoiles 8, Louvain-la-Neuve 1348, Belgium

^e WEL Research Institute, Avenue Pasteur 6, 1300 Wavre, Belgium

^f High Entropy Materials Center, National Tsing Hua University, 101, Sec. 2, Kuang-Fu Road, Hsinchu 30013, Taiwan

ARTICLE INFO

Keywords:

Refractory high entropy alloys
Oxidation resistance
AI model

ABSTRACT

Refractory high-entropy alloys (RHEAs) and complex concentrated alloys (RCCAs) are vital for high-temperature applications beyond the capabilities of Ni-based superalloys. Traditional methods for predicting oxidation resistance in these alloys are often inaccurate and resource-intensive. This study introduces a novel approach using Gradient Boosted Decision Trees (GBDT), an artificial intelligence technique, to predict specific mass gain due to oxidation. Utilizing a dataset synthesized from extensive literature and characterized by diverse alloy compositions and oxidation conditions, the model was trained using Iterated Nested k-fold Cross Validation with Shuffling (INKCVS). Our findings demonstrate that the GBDT model achieves a good balance between accuracy and generalization capacity in predicting oxidation resistance, as validated experimentally with selected alloys. This approach not only enhances prediction accuracy but also significantly reduces the need for extensive experimental testing, facilitating rapid development of new high-performance materials.

Refractory high-entropy alloys (RHEAs) [1], refractory complex concentrated alloys (RCCAs) and high entropy superalloys (HESAs) [2] have emerged as significant candidates for high-temperature applications, offering promising alternatives to conventional Ni-based superalloys, which are reaching their operational temperature limits. As future technologies demand materials that can endure higher temperatures, for applications such as aerospace engines, nuclear reactors, and thermal protection systems, the development of alloys capable of performing under such extreme conditions has become crucial. RHEAs and RCCAs, characterized by a mix of multiple principal refractory elements, often display superior mechanical properties and higher melting points compared to traditional materials [3,4]. These alloys, drawn from a palette of nine refractory metals including Zr, Hf, V, Nb, Ta, Cr, Mo, W, and Re, with minor additions of Al, Si, or Ti, are designed to withstand temperatures well beyond the 1000 °C threshold, competing with Ni-based superalloys.

Despite their high-temperature mechanical performance, a

significant challenge in the development of RHEAs and RCCAs is their susceptibility to oxidation [5–9], a critical factor in many high-temperature environments, which can severely impair their mechanical properties. Such a high temperature oxidation process is governed by complex thermodynamic and kinetic factors that involve the formation, growth, dissolution, and spalling of oxide layers. Traditionally, predicting the oxidation behavior of alloys has relied on empirical observations and complex physical models, which are both resource-intensive and limited in their predictive accuracy, particularly for new alloy compositions. These methods often fail to effectively navigate the vast design space required for developing innovative materials. Given these significant limitations, there is a pressing need for more adaptive and scalable models.

Recognizing the limitations of traditional methods, we propose a novel AI-driven approach to predict the oxidation resistance of RHEAs/RCCAs. Unlike conventional empirical or thermo-kinetic models, our AI techniques efficiently analyze extensive datasets to uncover patterns not

^{**} Corresponding author at: ICMCB, 87 avenue du Docteur Schweitzer, 33608 Bordeaux, France.

^{*} Corresponding author at: Department of Materials Science and Engineering, National Tsing Hua University, 101, Sec. 2, Kuang-Fu Road, Hsinchu 30013, Taiwan.

E-mail addresses: stephane.gorsse@icmcb.cnrs.fr (S. Gorsse), yehac@mx.nthu.edu.tw (A.-C. Yeh).

readily apparent through standard methods. By integrating AI, we aim to provide a more precise, less resource-demanding, and scalable solution, enabling the rapid evaluation of new alloys. Our method uniquely determines the specific mass gain, a critical metric for assessing oxidation resistance, based on alloy composition, exposure time, and temperature. This parameter is also relatively easy to measure experimentally using standard methods such as thermogravimetric analysis (TGA), making it a common choice in studies focusing on oxidation resistance. Consequently, specific mass gain is the most frequently reported property in the literature on the oxidation resistance of metals, making it particularly suitable for a machine learning approach. Compared to the study referenced in Ref. [10], which explored a limited compositional space resulting in fewer than 10,000 alloy combinations, our approach considers a broader range of over 10 million potential compositions. These extensive exploration and predictive capabilities offer the potential to rapidly pinpoint materials with optimal properties for high-temperature applications, significantly accelerating material development.

AI models rely on the data used for training, which must accurately link descriptive features of the alloy's chemistry and environmental conditions to metrics indicative of oxidation resistance. Unlike properties that depend solely on structure and can be predicted with high-throughput density functional theory (DFT), the oxidation behavior of

alloys necessitates a complex understanding of elemental diffusion, microstructure, oxide stability, and environmental interactions. Consequently, since a large computational database does not exist for this property, we must rely entirely on experimental data, which are often scarce and noisy. Therefore, our primary focus was to train an AI model that is both robust and generalizable despite such limitations.

To implement this solution, we first created a comprehensive experimental dataset extracted from the published literature [8,9,11–70]. This dataset (Fig. 1) encompasses both conventional refractory alloys and RHEAs/RCCAs composed from a palette of 11 elements: Al, Cr, Hf, Mo, Nb, Si, Ta, Ti, V, W, and Zr. It details alloy composition, oxidation test temperatures, and exposure times. These descriptors are controllable during the alloy's fabrication and thus chosen as input features for our AI model. The target output is the measured specific mass gain during oxidation, Δm^* , i.e., the increase in mass per unit area of an alloy due to the formation of oxide layers when exposed to air at elevated temperatures. With 886 observations, the dataset provides a fair basis for training our predictive model. While most of the papers selected for our dataset involve thermogravimetric analysis (TGA), we acknowledge that variations due to specific equipment and slight differences in practice by different research teams can introduce noise into the data. Despite these variations, our model is designed to provide a direct and efficient means of predicting the specific mass gain during

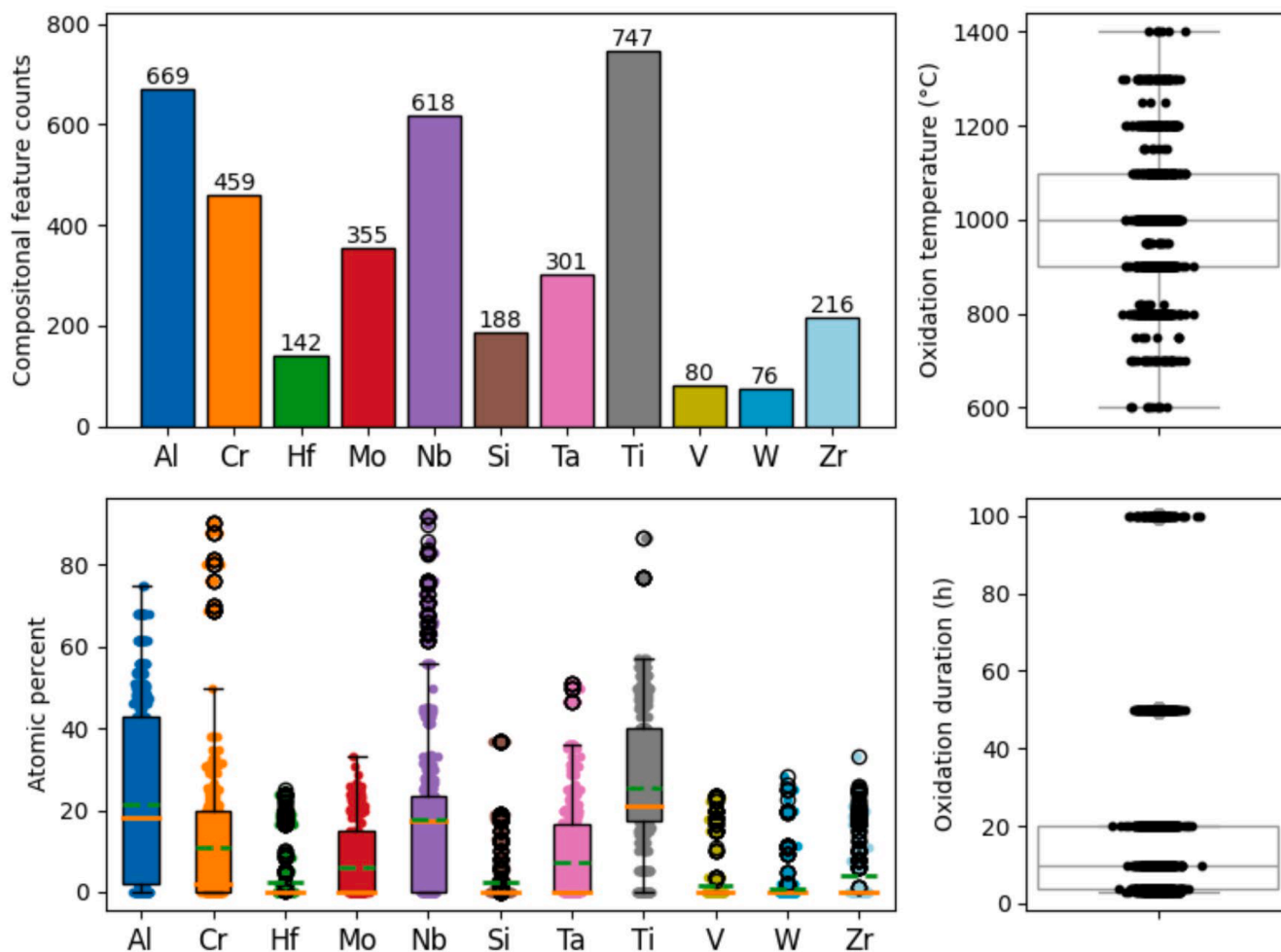


Fig. 1. Distribution of compositional and processing features in the dataset. The bar chart in the upper left panel displays the number of observations containing each element, while the boxplots in the lower left panel show the concentration distributions across all alloys in the dataset. The interquartile ranges (IQR = Q3 - Q1), where Q3 is the third quartile marking the 75th percentile and Q1 is the first quartile marking the 25th percentile, are illustrated by the boxes, with median values indicated by red lines and mean values by green dashed lines. Whiskers on the boxplots extend to the furthest point within 1.5 times the IQR from the upper and lower quartiles, showing the range of typical data points. Outliers are depicted as individual points. The boxplot in the upper right panel shows the distribution of oxidation temperatures. The boxplot in the lower right panel shows the distribution of oxidation duration.

high-temperature exposure, utilizing controllable alloy fabrication parameters (elemental composition) and exposure environment (temperature and time) to offer rapid and reliable evaluations for material designers and experimentalists.

Fig. 2 presents a compositional similarity network of alloys, which allows for the visual exploration of relationships between different alloy compositions in our dataset. Each of the 163 nodes in the graph represents a unique alloy, identified by a distinct composition. The color of each node indicates the element most concentrated by molar percentage. Edges connect alloys exhibiting significant similarity, based on cosine similarity, which is calculated by comparing the normalized composition vectors of the alloys to assess their relative orientation in the hyper-dimensional composition space. The color of each edge is determined by the predominant element in the average composition of the two connected alloys. This average is obtained by calculating the mean concentrations of each element and selecting the element with the highest concentration. This edge coloring method allows for quick identification of the dominant element in the connections between

different alloys. The positions of the nodes result from the balance between repulsive forces among all nodes and the attractive forces of the edges, which depend on the weight of the similarity. Consequently, clusters of densely interconnected nodes emerge, indicating that alloys within these groups share marked similarities. Three areas with high concentrations of blue, orange, and violet colors indicate regions of the compositional space where Al, Cr, and Nb frequently dominate. A central area with a low density of nodes reveals less explored regions in the alloy composition space, suggesting domains of compositions that have not been extensively studied. To enrich our dataset, we randomly sampled 9 compositions from this region, synthesized these 9 so-called "random" alloys by arc-melting, and measured the temporal evolution of their specific mass gain under air at 1000 °C for up to 50 h using Thermogravimetric Analysis (TGA). The results are reported (Fig. 2) as black nodes, whose diameter is proportional to the observed mass gain, together with the surface condition of the random alloys after 20 h of oxidation at 1000 °C. These experimental results will be presented in detail and discussed in a subsequent article. Four of these random alloys

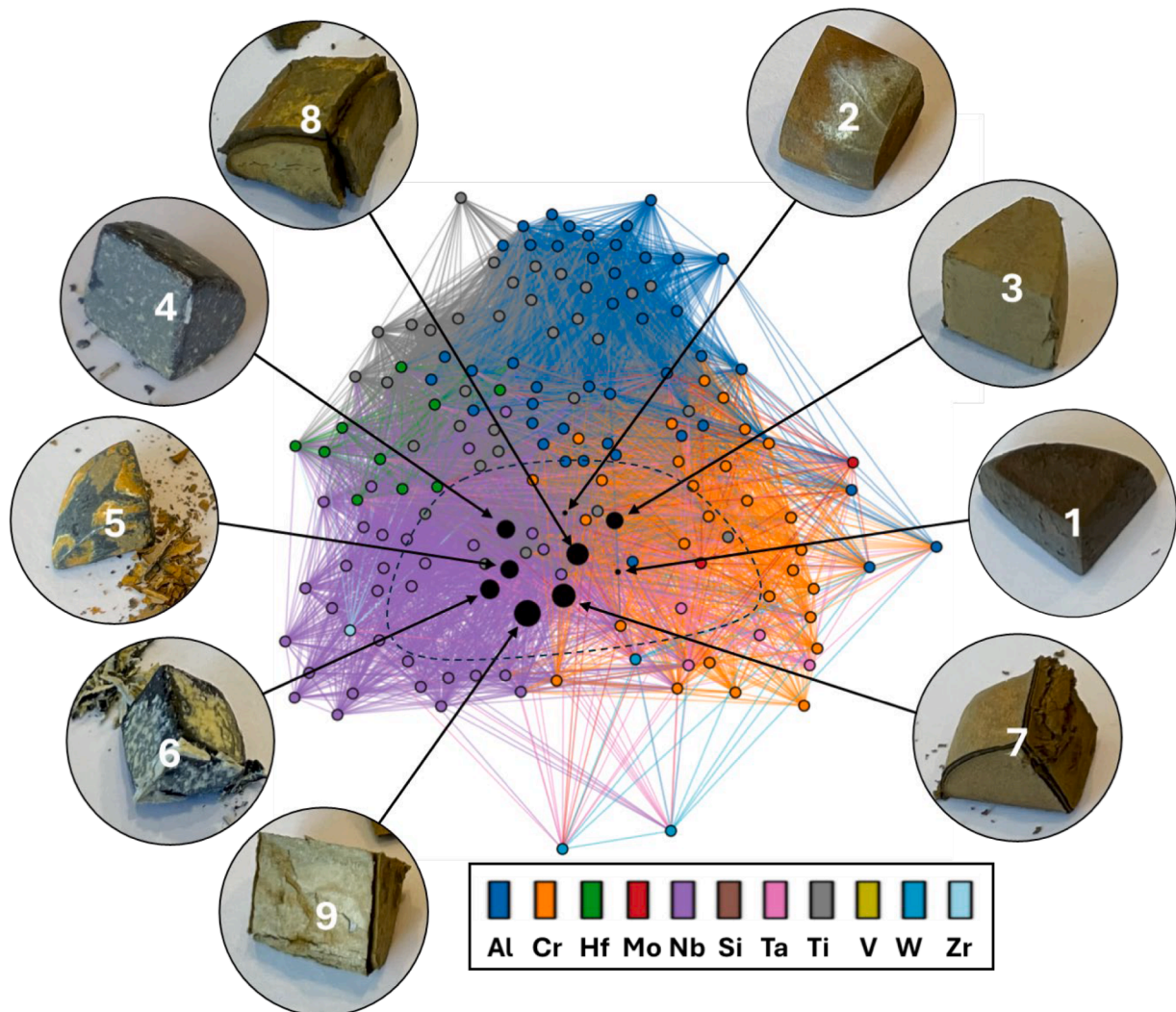


Fig. 2. Compositional similarity network of alloys. This network graph, created using the NetworkX [71] Python library, visualizes relationships between 163 distinct alloy compositions in our database, each represented by a node color-coded by the predominant element in molar percentage. Connections between nodes, or edges, are colored based on the dominant element in their average composition, determined by cosine similarity of normalized composition vectors. This similarity measures how closely related the alloys are in the hyper-dimensional composition space. Clusters of densely interconnected nodes illustrate groups of alloys with significant similarities, while a central area with fewer nodes highlights less explored compositional regions. Notably, black nodes with diameters proportional to the observed mass gain represent nine alloys randomly sampled and tested for this study (1: $\text{Al}_{0.5}\text{CrMoNbTi}$, 2: $\text{Al}_{0.5}\text{CrMoNbTaTi}$, 3: $\text{Al}_{0.5}\text{CrNbTaTiZr}$, 4: $\text{Al}_{0.5}\text{NbTaTi}$, 5: $\text{Cr}_{0.25}\text{NbTaTi}$, 6: NbTaTi , 7: CrNbTaTiZr , 8: $\text{Al}_{0.5}\text{Cr}_1\text{Nb}_{1.5}\text{Ta}_2\text{Ti}_1\text{Zr}_{0.5}$, 9: $\text{Cr}_{0.5}\text{Nb}_1\text{Ta}_{1.3}\text{Ti}_{0.6}\text{Zr}_{0.3}$). The inset photographs depict the surface condition of these alloys after 20 h of oxidation in air at 1000 °C.

were included in the training dataset, while the remaining five were used to test the model for a supplementary evaluation on previously unseen data. These will be referred to as “test alloys” in what follows.

Due to the relatively small size of the dataset and the complexity of the property to be modeled, we selected the XGBoost (Extreme Gradient Boosting) machine learning algorithm [72], an advanced implementation of gradient-boosted decision trees (GBDT) particularly effective at managing non-linear relationships and feature interactions. Compared to simpler models such as multivariate linear regression (MLR) and more complex models like neural networks, which often overfit unless provided with large datasets, XGBoost offers a balanced solution. It maintains model simplicity while handling effectively our dataset of 886 observations and 13 features. These features include 11 elemental concentrations (the palette of elements found in RHEAs: Al, Cr, Hf, Mo, Nb, Si, Ta, Ti, V, W, and Zr) as well as the time and temperature of isothermal oxidation exposure under air, as these variables are critical for accurately predicting oxidation resistance in RHEAs. The selection ensures a comprehensive representation of the chemical and operational conditions affecting oxidation outcomes, specifically the specific mass gain.

To enhance our model training and evaluation, we implemented Iterated Nested k-fold Cross Validation with Shuffling (INKCVS) [73]. This method is particularly effective in hyperparameter optimization, rigorous model selection, robustness assessment, and evaluating generalization capabilities. Hyperparameters, which are predefined settings that are derived during training, play a critical role as they influence the training process and must be carefully selected and tuned to optimize performance. We tailored several XGBoost hyperparameters to better suit our dataset’s specific challenges. Adjustments included reducing tree depth to prevent excessive complexity and overfitting, increasing the node creation threshold to improve generalization, and using partial data sampling to enhance tree diversity and reduce overfitting risks.

Nested k-fold Cross Validation (NKCVC) involves two levels: an inner loop for model training and hyperparameter tuning, and an outer loop for validating the model’s performance. This structure not only enhances standard cross-validation by adding an additional level of validation to prevent overfitting to a single data subset but also provides a more reliable estimate of the model’s ability to generalize to new data. Configured with 5 splits in the inner loop and 4 splits in the outer loop, our setup minimizes data leakage and overfitting by ensuring unbiased evaluations based on multiple, independent tests across the dataset.

Shuffling the dataset before each iteration mitigates any bias from inadvertent patterns in the data order, thereby enhancing the robustness of evaluations. Iterating this process 25 times allows each input row to contribute to 100 predictions (4-fold out CV times 25 interactions), facilitating a detailed computation of residuals and the standard deviation of predictions for each input. We chose the mean absolute error (MAE) as our evaluation metric for its resistance to outliers—preventing extreme values from disproportionately skewing the results—and for its straightforward interpretation. To prevent bias toward features with larger scales, we normalized the data using the Standard Scaler, which standardizes features by removing the mean and scaling to unit variance.

Fig. 3 illustrates the predictive accuracy of the Gradient Boosted Decision Trees (GBDT) model by comparing the actual versus predicted specific mass gains, $\ln(\Delta m^*)$, for each of the 861 unique observations, which include specific alloy compositions, temperatures, and oxidation durations. A dashed 1:1 line indicates perfect agreement. The model’s effectiveness is evaluated using MAE and standard deviation, calculated over all predictions from the 100 models generated during the INKCVS. These metrics are averaged over all predictions made by the 100 models for each observation in the databases. Additionally, predictions on the 5 test alloys, comprising 25 observations, are depicted with black dots with red edges. Although the average MAE for unseen data is slightly higher than for INKCVS, the model effectively infers the target property

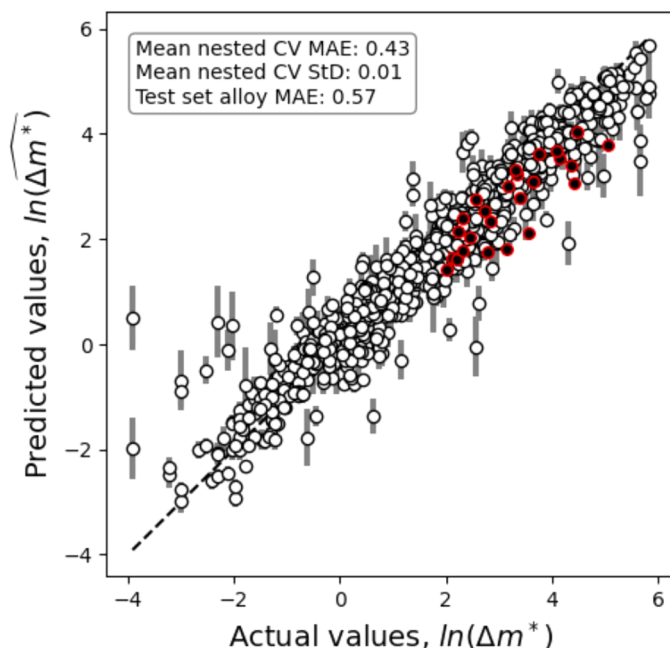


Fig. 3. Accuracy of the Gradient Boosted Decision Trees (GBDT) model in predicting specific mass gain due to oxidation in air between 600–1400 °C and over durations ranging from 3 to 100 h, as determined through Iterated Nested K-fold Cross Validation with Shuffling (INKCVS). Each of the 861 data point represents a unique combination of alloy composition, temperature, and oxidation duration. The mean absolute error (MAE) and standard deviation from INKCVS are displayed. Additionally, MAE for the unseen test set of 5 random alloys (black dots with red edges representing 25 observations), calculated from the residuals between predicted and actual values, is also shown.

with significant accuracy, demonstrating strong generalization capabilities.

This rigorous approach ensures the selection of the best model from among the 100 that were trained during the INKCVS, with finely tuned hyperparameters, making the model robust and capable of generalizing well. The optimal model underwent a final round of training on the entire dataset, now including 886 observations, to ensure its full optimization. Fig. 4 compares these results with those of a multivariate linear regression (MLR) model trained on the same dataset. Performance metrics such as the coefficient of determination (R^2), root mean squared error (RMSE), and MAE highlight the superior performance of the GBDT model compared to the MLR model.

SHAP (SHapley Additive exPlanations) [74] values are used to analyze and visualize the impact of various features on model predictions. Initially, the correlation coefficient between the SHAP values and the actual feature values is calculated to determine if a feature’s influence on the target is positive or negative. To quantify the overall importance of each feature, the absolute average of their SHAP values is computed. These results are visualized in a horizontal bar chart (Fig. 5), where features impacting the model positively are indicated in red and those with a negative impact are shown in blue. This visualization highlights the most influential features affecting specific mass gain. Ranked by importance, they include oxidation temperature, Nb concentration, oxidation time, and Al concentration. Notably, oxidation temperature and time, along with concentrations of Nb, Zr, V, Ti, W, and Hf, positively correlate with an increase in specific mass gain, indicating a detrimental effect on oxidation resistance. Conversely, increases in Al, Mo, Cr, Ta, and Si concentrations lead to a decrease in specific mass gain, enhancing oxidation resistance.

From a physical standpoint, the formation of thermodynamically stable oxides like Al_2O_3 [75], Cr_2O_3 [76], and SiO_2 [77], which exhibit

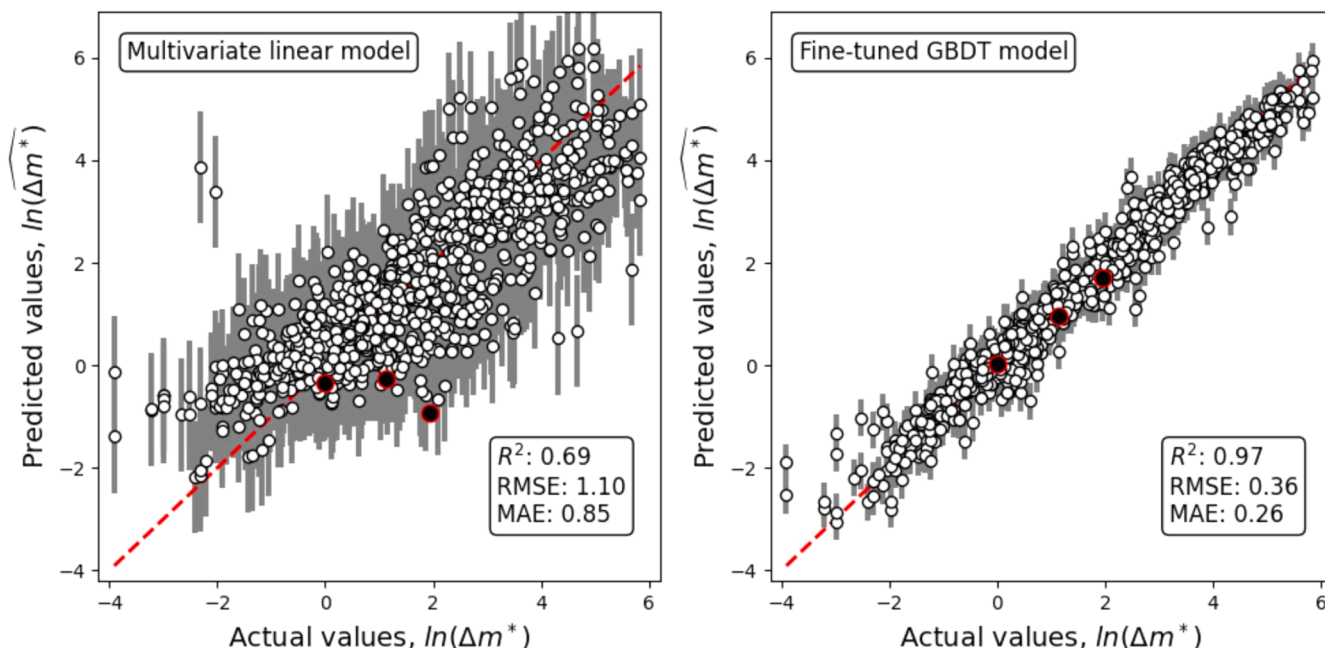


Fig. 4. Comparison of the best Gradient Boosted Decision Trees (GBDT) model and a Multivariate Linear Regression model in predicting specific mass gain due to oxidation in air between 600–1400 °C and over durations ranging from 3 to 100 h, after retraining with the entire dataset. Each of the 886 data points represents a unique combination of alloy composition, temperature, and oxidation duration. For each model, the mean absolute error (MAE), root mean squared error (RMSE), and coefficient of determination (R^2) are depicted. These metrics are calculated based on the residuals between the predicted and actual values. The three black dots with red edges represent a final experimental validation of the model's predictions.

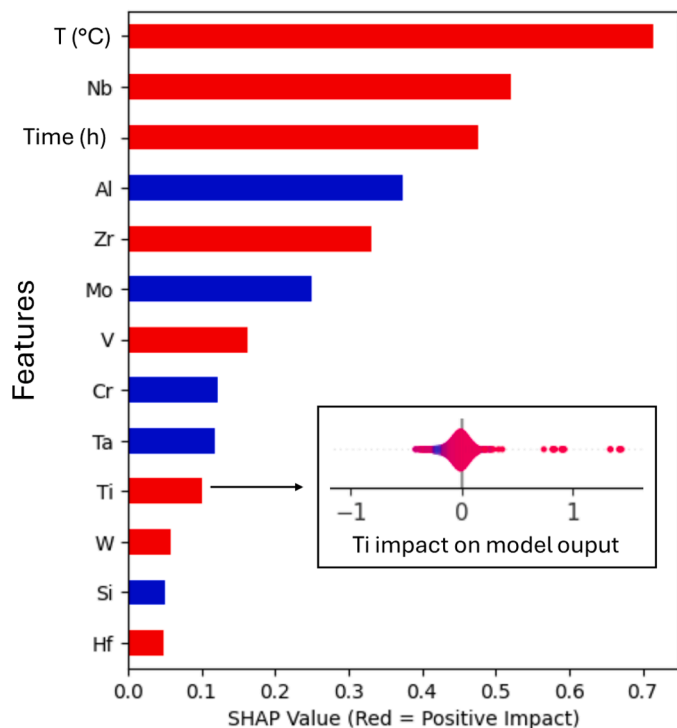


Fig. 5. Impact of model features on specific mass gain prediction. Average SHAP values for model features in predicting specific mass gain, ordered by descending importance. Bars are colored to indicate the nature of each feature's impact on predictions: red for positive and blue for negative influences. Inset figure shows the positive and negative relationships of the Ti concentration with specific mass gain.

low oxygen permeability, in Al, Cr, or Si-bearing RHEAs, explains the positive impact of these elements on oxidation resistance. In contrast, the addition of Zr and V has been found to degrade oxidation resistance due to the formation of non-protective oxides or promoting internal oxidation [7]. Conversely, Ta-containing alloys, such as TaMoCrTiAl [8] and $\text{Al}_{18}\text{Si}_3\text{Ti}_5\text{Cr}_{25}\text{Nb}_{15}\text{Mo}_{20}\text{Ta}_{13}$ [9], benefit from the formation of CrTaO_4 , a complex protective oxide layer. However, Nb's presence in alloys such as NbMoCrTiAl [8] tends to reduce resistance, leading to the development of porous Nb_2O_5 scales that facilitate severe oxide spallation. Titanium presents a more nuanced case. While the SHAP analysis indicates that increasing the Ti level generally results in heightened mass gain—suggesting a negative impact on oxidation resistance—literature points to beneficial effects in specific contexts. For instance, Ti supports the formation of protective CrTaO_4 layers [6], and its presence in small quantities within certain RCCA formulations leads to the formation of rutile-type complex oxides that improve overall resistance [7]. This paradoxical behavior of titanium is captured in our model's nuanced analysis, as depicted in the inset of Fig. 5, where Ti can enhance the oxidation resistance when used in low concentration.

This detailed understanding of how various elements influence the oxidation resistance of RHEAs and RCCAs informs the design of future alloys optimized for high-temperature performance. Our AI model's predictions, aligning with these experimental findings, confirm its accuracy and reliability. This synergy between experimental results and AI predictions underscores the model's effectiveness in reflecting real-world alloy behavior under high-temperature conditions, thus serving as a crucial tool for alloy composition optimization.

For a final and rapid validation, we utilized our fine-tuned GBDT model to explore the target space for specific mass gain values of 1, 3 and 7 mg/cm^2 . We focused on the quinary system Al-Cr-Mo-Ta-Ti, with each component adjusted in 5 % compositional steps. From the inferences, we selected the compositions $\text{Al}_{30}\text{Cr}_{25}\text{Mo}_{20}\text{Ta}_{15}\text{Ti}_{10}$, $\text{Al}_{30}\text{Cr}_{30}\text{Mo}_{20}\text{Ta}_{15}\text{Ti}_{15}$, and $\text{Al}_{30}\text{Cr}_{30}\text{Mo}_{30}\text{Ta}_{15}\text{Ti}_{15}$, produced them via arc-melting, and then measured their specific mass gains during a 20 h oxidation test in air at 1000 °C. The results are depicted in Fig. 4 as black dots with red edges. While they can lie far from the 1:1 line for the multivariate linear model,

they closely align with the 1:1 line for our fine-tuned GBDT model, indicating strong agreement between predicted and observed outcomes. This successful experimental validation of the GBDT model's predictions, alongside comparisons to simpler a model, confirms the model's effectiveness in efficiently mapping the design space. Furthermore, this validation also serves as a practical demonstration of our model's application. Looking ahead, we plan to integrate this model with other AI-models previously developed for assessing high-temperature strength and room temperature ductility of refractory high-entropy alloys [78]. This integration aims to comprehensively map the three-dimensional Pareto front, delineating the trade-offs between these mechanical properties and high-temperature oxidation resistance, thus extending our model's utility beyond this study.

In summary, we developed an experimental database with 886 observations on oxidation mass gain in RHEAs, now available in the supplementary materials. Despite potential biases and noise in this experimental dataset, our Gradient Boosted Decision Trees model effectively predicts specific mass gain using alloy composition (including elements like Al, Cr, Hf, Mo, Nb, Si, Ta, Ti, V, W, and Zr), and oxidation conditions (temperature and duration). This model balances accuracy with generalization, proving invaluable in early material design stages by enabling rapid evaluations to eliminate unsuitable materials and identify promising ones. This facilitates quicker, more focused resource allocation in materials research. We acknowledge that specific mass gain captures only one facet of oxidation resistance. Quantifying oxidation resistance through a single value can be complex as it might encompass both mass gain from oxide formation and mass loss due to spallation or vaporization. To address these complexities, future work could explore the application of the Pilling-Bedworth ratio [79], which assesses the volume changes of oxide formations relative to the original metal and would complement our approach by enhancing the overall understanding of oxidation behavior.

CRedit authorship contribution statement

Stéphane Gorsse: Writing – original draft, Visualization, Validation, Supervision, Software, Resources, Project administration, Methodology, Investigation, Funding acquisition, Formal analysis, Data curation, Conceptualization. **Wei-Chih Lin:** Investigation, Data curation. **Hideyuki Murakami:** Writing – review & editing, Investigation. **Gian-Marco Rignanese:** Writing – review & editing, Validation. **An-Chou Yeh:** Writing – review & editing, Supervision, Resources, Project administration, Funding acquisition.

Declaration of competing interest

The authors declare that they have no known competing financial interests or personal relationships that could have appeared to influence the work reported in this paper.

Acknowledgments

This work has benefited from a government grant managed by the Agence Nationale de la Recherche under the France 2030 program; reference ANR-22-PEXD-0003.

SG, WCL, and GMR gratefully acknowledge the support of the CNRS through the IRP MALCOM initiative.

WCL acknowledges the support from the 80|Prime program of the Mission for Transversal and Interdisciplinary Initiatives (MITI) for funding his doctoral research through the 'multi-team interdisciplinary research projects' grant.

We also thank Louis Moreau for his assistance with the thermogravimetric analysis measurements.

References

- [1] O.N. Senkov, et al., Refractory high-entropy alloys, *Intermetallics* 18 (9) (2010) 1758–1765 (Barking).
- [2] A.C. Yeh, et al., Developing new type of high temperature alloys–high entropy superalloys, *Int. J. Metall. Mater. Eng.* 1 (1) (2015).
- [3] S. Gorsse, D.B. Miracle, O.N. Senkov, Mapping the world of complex concentrated alloys, *Acta Mater.* 135 (2017) 177–187.
- [4] O.N. Senkov, S. Gorsse, D.B. Miracle, High temperature strength of refractory complex concentrated alloys, *Acta Mater.* 175 (2019) 394–405.
- [5] B.R. Anne, et al., A crucial review on recent updates of oxidation behavior in high entropy alloys, *SN Appl. Sci.* 3 (3) (2021).
- [6] P. Kumar, et al., Recent progress in oxidation behavior of high-entropy alloys: a review, *APL Mater.* 10 (12) (2022).
- [7] K.C. Lo, et al., Elemental effects on the oxidation of refractory compositionally complex alloys, *Int. J. Refract. Met. Hard Mater.* 108 (2022).
- [8] F. Müller, et al., On the oxidation mechanism of refractory high entropy alloys, *Corros. Sci.* 159 (2019).
- [9] K.C. Lo, et al., An oxidation resistant refractory high entropy alloy protected by CrTaO(4)-based oxide, *Sci. Rep.* 9 (1) (2019) 7266.
- [10] D. Saucedo, et al., High throughput exploration of the oxidation landscape in high entropy alloys, *Mater. Horiz.* 9 (10) (2022) 2644–2663.
- [11] M.P. Brady, P.F. Tortorelli, L.R. Walker, Correlation of alloy microstructure with oxidation behavior in chromia-forming intermetallic-reinforced Cr alloys, *Mater. High Temp.* 17 (2) (2014) 235–241.
- [12] Y. Umakoshi, et al., Oxidation resistance of intermetallic compounds Al₃Ti and TiAl, *J. Mater. Sci.* 24 (5) (1989) 1599–1603.
- [13] D.B. Lee, Effect of Cr, Nb, Mn, V, W and Si on high temperature oxidation of TiAl alloys, *Met. Mater. Int.* 11 (2) (2005) 141–147.
- [14] M. Schmitz-Niedermaier, M. Schütze, The Oxidation Behavior of Several Ti–Al Alloys at 900 °C in Air, *Oxid. Met.* 52 (3/4) (1999) 225–240.
- [15] P. Pérez, et al., The Influence of the Alloy Microstructure on the Oxidation Behavior of Ti–46Al–1Cr–0.2Si Alloy, *Oxid. Met.* 53 (1/2) (2000) 99–124.
- [16] H. Guleryuz, H. Cimenoglu, Oxidation of Ti–6Al–4V alloy, *J. Alloys Compd.* 472 (1–2) (2009) 241–246.
- [17] S. Burk, et al., High-temperature oxidation behaviour of a single-phase (Mo,Ti)₅Si₃ (Mo–Si–Ti) alloy, *Scr. Mater.* 66 (5) (2012) 223–226.
- [18] O.N. Senkov, et al., Oxidation behavior of a refractory NbCrMo_{0.5}Ta_{0.5}TiZr alloy, *J. Mater. Sci.* 47 (18) (2012) 6522–6534.
- [19] B. Gorr, et al., High temperature oxidation behavior of an equimolar refractory metal-based alloy 20Nb 20Mo 20Cr 20Ti 20Al with and without Si addition, *J. Alloys Compd.* 688 (2016) 468–477.
- [20] T.M. Butler, et al., High temperature oxidation behaviors of equimolar NbTiZrV and NbTiZrCr refractory complex concentrated alloys (RCCAs), *J. Alloys Compd.* 729 (2017) 1004–1019.
- [21] B. Gorr, et al., High-temperature oxidation behavior of refractory high-entropy alloys: effect of alloy composition, *Oxid. Met.* 88 (3–4) (2017) 339–349.
- [22] T.M. Butler, K.J. Chaput, Native oxidation resistance of Al₂₀Nb₃₀Ta₁₀Ti₃₀Zr₁₀ refractory complex concentrated alloy (RCCA), *J. Alloys Compd.* 787 (2019) 606–617.
- [23] F. Müller, et al., Effect of microalloying with silicon on high temperature oxidation resistance of novel refractory high-entropy alloy Ta–Mo–Cr–Ti–Al, *Mater. High Temp.* 35 (1–3) (2017) 168–176.
- [24] R. Gawel, L. Rogal, K. Przybylski, Oxidation Resistance of Ti–Al–Cr–Nb-Based High-Entropy Alloys in Air at 1073 K, *J. Mater. Eng. Perform.* 28 (7) (2019) 4163–4170.
- [25] D. Pilone, F. Felli, A. Brotzu, High temperature oxidation behaviour of TiAl–Cr–Nb–Mo alloys, *Intermetallics* 43 (2013) 131–137. (Barking).
- [26] S. Schellert, et al., The effect of Al on the formation of a CrTaO₄ layer in refractory high entropy alloys Ta–Mo–Cr–Ti–xAl, *Oxid. Met.* 96 (3–4) (2021) 333–345.
- [27] Y. Li, et al., Improvement of “pest” oxidation resistance of Nb–Mo–W–Zr solid-solution alloy at 800 °C by gas nitridation, *Corros. Sci.* 187 (2021).
- [28] J. Geng, P. Tsakiroopoulos, G. Shao, Oxidation of Nb–Si–Cr–Al *in situ* composites with Mo, Ti and Hf additions, *Mater. Sci. Eng. A* 441 (1–2) (2006) 26–38.
- [29] N. Yurchenko, et al., Oxidation behavior of refractory AlNbTiVZr(0.25) High-Entropy Alloy, *Materials* 11 (12) (2018). (Basel).
- [30] O. Hernandez-Negrete, P. Tsakiroopoulos, On the microstructure and isothermal oxidation at 800, 1200, and 1300 °C of the Al-25.5Nb-6Cr-0.5Hf (at%) alloy, *Materials* 12 (16) (2019). (Basel).
- [31] K.C. Lo, et al., Oxidation behaviour of a novel refractory high entropy alloy at elevated temperatures, *Intermetallics* 119 (2020). (Barking).
- [32] D. Qiao, et al., The mechanical and oxidation properties of novel B2-ordered Ti₂ZrHf_{0.5}VNb_{0.5}Al_x refractory high-entropy alloys, *Mater. Charact.* 178 (2021).
- [33] S. Lu, et al., Effect of Y additions on the oxidation behavior of vacuum arc melted refractory high-entropy alloy AlMo_{0.5}NbTa_{0.5}TiZr at elevated temperatures, *Vacuum* 201 (2022).
- [34] Y. Lin, et al., Effects of vanadium content on the high temperature oxidation behavior of NbTiZrAlV refractory complex concentrated alloys, *J. Alloys Compd.* 905 (2022).
- [35] N.J. Welch, et al., High-temperature oxidation behavior of TaTiCr, Ta₄Ti₃Cr, Ta₂TiCr, and Ta₄TiCr₃ concentrated refractory alloys, *J. Alloys Compd.* 941 (2023).
- [36] Y. Yan, et al., The oxidation-resistance mechanism of WTa₂NbTiAl refractory high entropy alloy, *Corros. Sci.* 204 (2022).
- [37] J. Jayaraj, et al., Microstructure, mechanical and thermal oxidation behavior of AlNbTiZr high entropy alloy, *Intermetallics* 100 (2018) 9–19. (Barking).

- [38] Y. Murayama, S. Hanada, High temperature strength, fracture toughness and oxidation resistance of Nb–Si–Al–Ti multiphase alloys, *Sci. Technol. Adv. Mater.* 3 (2) (2018) 145–156.
- [39] K. Chattopadhyay, R. Mitra, K.K. Ray, Nonisothermal and isothermal oxidation behavior of Nb–Si–Mo alloys, *Metall. Mater. Trans. A* 39 (3) (2008) 577–592.
- [40] O.N. Senkov, J. Gild, T.M. Butler, Microstructure, mechanical properties and oxidation behavior of NbTaTi and NbTaZr refractory alloys, *J. Alloys. Compd.* 862 (2021).
- [41] M.d.P. Moricca, S.K. Varma, Isothermal oxidation behaviour of Nb–W–Cr Alloys, *Corros. Sci.* 52 (9) (2010) 2964–2972.
- [42] S. Zhang, R. Li, Y. Xu, Zr alloying effects on the microstructure, compression performance and oxidation resistance of refractory high entropy alloys, *Mater. Res. Express.* 9 (9) (2022).
- [43] S. Lu, et al., Effect of V and Ti on the oxidation resistance of WMoTaNb refractory high-entropy alloy at high temperatures, *Basel, Metals* 12 (1) (2021).
- [44] X. Li, et al., The determining role of Al addition on tribology properties and oxidation behavior at elevated temperatures of TiZrHfNb refractory high-entropy alloy, *Mater. Charact.* 189 (2022).
- [45] S. Lu, et al., Effect of Al content on the oxidation behavior of refractory high-entropy alloy AlMo0.5NbTa0.5TiZr at elevated temperatures, *Int. J. Refract. Met. Hard Mater.* 105 (2022).
- [46] Y. Du, et al., Effect of Y on the high-temperature oxidation behavior of CrMoTaTi refractory high entropy alloy, *Int. J. Refract. Met. Hard Mater.* 103 (2022).
- [47] A. Ostovari Moghaddam, et al., High temperature oxidation resistance of W-containing high entropy alloys, *J. Alloys Compd.* 897 (2022).
- [48] R. Zhang, et al., Oxidation resistance properties of refractory high-entropy alloys with varied AlxCrTiMo content, *J. Mater. Sci.* 56 (4) (2020) 3551–3561.
- [49] L.C. Li, et al., Enhanced oxidation resistance of MoTaTiCrAl high entropy alloys by removal of Al, *Sci. China Mater.* 64 (1) (2020) 223–231.
- [50] B.G. Kim, G.M. Kim, C.J. Kim, Oxidation behavior of TiAl–X (X = Cr, V, Si, Mo or Nb) intermetallics at elevated temperature, *Scr. Metall. Mater.* 33 (7) (1995) 1117–1125.
- [51] L.L. Zhao, et al., Influence of Y addition on the long time oxidation behaviors of high Nb containing TiAl alloys at 900 °C, *Intermetallics* 18 (8) (2010) 1586–1596. (Barking).
- [52] G. Chen, Z. Sun, X. Zhou, Oxidation and mechanical behavior of intermetallic alloys in the Ti–Nb–Al ternary system, *Mater. Sci. Eng. A* 153 (1–2) (1992) 597–601.
- [53] C.T. Liu, et al., Effects of alloy additions on the microstructure and properties of CrCr2Nb alloys, *Mater. Sci. Eng. A* 214 (1–2) (1996) 23–32.
- [54] L. Su, et al., Improvement in the oxidation resistance of Nb–Ti–Si–Cr–Al–Hf alloys containing alloyed Ge and B, *Corros. Sci.* 88 (2014) 460–465.
- [55] C.M. Liu, et al., Microstructure and oxidation behavior of new refractory high entropy alloys, *J. Alloys Compd.* 583 (2014) 162–169.
- [56] O.A. Waseem, H.J. Ryu, Combinatorial synthesis and analysis of AlxTayVz-Cr20Mo20Nb20Ti20Zr10 and Al10CrMoxNbTiZr10 refractory high-entropy alloys: oxidation behavior, *J. Alloys Compd.* 828 (2020).
- [57] Y.K. Cao, et al., Effects of Al and Mo on high temperature oxidation behavior of refractory high entropy alloys, *Trans. Nonferrous Met. Soc. China* 29 (7) (2019) 1476–1483.
- [58] P. Zhang, et al., Oxidation response of a vacuum arc melted NbZrTiCrAl refractory high entropy alloy at 800–1200 °C, *Vacuum* 162 (2019) 20–27.
- [59] C.H. Chang, M.S. Titus, J.W. Yeh, Oxidation behavior between 700 and 1300 °C of refractory TiZrNbHfTa high-entropy alloys containing aluminum, *Adv. Eng. Mater.* 20 (6) (2018).
- [60] X. Yang, et al., Effect of Al content on the thermal oxidation behaviour of AlHfMoNbTi high-entropy alloys analysed by *in situ* environmental TEM, *Corros. Sci.* 191 (2021).
- [61] Z. An, et al., Simultaneously enhanced oxidation resistance and mechanical properties in a novel lightweight Ti2VZrNb0.5Al0.5 high-entropy alloy, *Sci. China Mater.* 65 (10) (2022) 2842–2849.
- [62] Y. Xiao, et al., Microstructure and oxidation behavior of the CrMoNbTaV high-entropy alloy, *J. Mater. Res.* 34 (2) (2018) 301–308.
- [63] G.T.J. Mayo, W.H. Shepherd, A.G. Thomas, Oxidation behaviour of niobium-chromium alloys, *J. Less Common Met.* 2 (2–4) (1960) 223–232.
- [64] T.M. Butler, et al., Oxidation behaviors of CrNb, CrNbTi, and CrNbTaTi concentrated refractory alloys, *Intermetallics* 140 (2022).
- [65] D. Ouyang, et al., Oxidation behavior of the Ti38V15Nb23Hf24 refractory high-entropy alloy at elevated temperatures, *Corros. Sci.* 198 (2022).
- [66] S. Schellert, et al., Formation of rutile (Cr,Ta,Ti)O2 oxides during oxidation of refractory high entropy alloys in Ta–Mo–Cr–Ti–Al system, *Corros. Sci.* (2023) 211.
- [67] N. Yurchenko, et al., Oxidation behaviour of eutectic refractory high-entropy alloys at 800–1000 °C, *Corros. Sci.* 205 (2022).
- [68] O.A. Waseem, et al., A combinatorial approach for the synthesis and analysis of AlxCrMozNbTiZr high-entropy alloys: oxidation behavior, *J. Mater. Res.* 33 (19) (2018) 3226–3234.
- [69] R. Romero, I.J. Beyerlein, C.V. Ramana, Microstructure and oxidation behavior of a CrMoNbTaW refractory high entropy alloy, *ACS Appl. Eng. Mater.* 1 (1) (2022) 132–139.
- [70] H. Zhang, et al., The as-cast AlxCrTaTi refractory medium entropy alloys with good room-temperature mechanical properties and high-temperature oxidation resistance, *J. Alloys Compd.* (2023) 932.
- [71] A. Aric, D.A.S.A.P.J.S. Hagberg, Exploring network structure, dynamics, and function using NetworkX, in: *Proceedings of the 7th Python in Science Conference (SciPy2008)*, Pasadena, CA USA, 2008.
- [72] T. Chen, C. Guestrin, XGBoost: a scalable tree boosting system, in: *Proceedings of the 22nd ACM SIGKDD International Conference on Knowledge Discovery and Data Mining*, New York, NY, USA, 2016.
- [73] D. Krstajic, et al., Cross-validation pitfalls when selecting and assessing regression and classification models, *J. Cheminform.* 6 (1) (2014) 10.
- [74] S.M. Lundberg, S. Lee, A unified approach to interpreting model predictions, *Neural Inf. Process. Syst.* (2017).
- [75] X.H. Wang, Y.C. Zhou, High-temperature oxidation behavior of Ti2AlC in Air, *Oxid. Met.* 59 (3/4) (2003) 303–320.
- [76] Y. Hua, et al., Laser shock processing effects on isothermal oxidation resistance of GH586 superalloy, *Appl. Surf. Sci.* 330 (2015) 439–444.
- [77] M.A. Azim, et al., Creep Resistance and Oxidation Behavior of Novel Mo–Si–B–Ti Alloys, *Jom* 67 (11) (2015) 2621–2628.
- [78] O.N. Senkov, et al., Correlations to improve high-temperature strength and room temperature ductility of refractory complex concentrated alloys, *Mater. Des.* 239 (2024).
- [79] C. Xu, W. Gao, Pilling-Bedworth ratio for oxidation of alloys, *Mater. Res. Innov.* 3 (2000) 231–235.